ADVANCES IN ATMOSPHERIC SCIENCES, VOL. 29, NO. 6, 2012, 1292–1304

Influence of a Southern Shift of the ITCZ from Quick Scatterometer Data on the Pacific North Equatorial Countercurrent

WU Fanghua[1,2,3] (吴方华), LIN Pengfei*[3] (林鹏飞), and LIU Hailong[3] (刘海龙)

[1]*Division of Climate System Modeling, National Climate Center, Beijing* 100081

[2]*State Key of Laboratory of Atmospheric Boundary Layer Physics and Atmospheric Chemistry, Institute of Atmospheric Physics, Chinese Academy of Sciences, Beijing* 100029

[3]*State Key Laboratory of Numerical Modeling for Atmospheric Sciences and Geophysical Fluid Dynamics, Institute of Atmospheric Physics, Chinese Academy of Sciences, Beijing* 100029

(Received 7 August 2011; revised 30 January 2012)

ABSTRACT

By analyzing the climatologically averaged wind stress during 2000–2007, it is found that the easterly wind stress in the northern tropical Pacific Ocean from Quick Scatterometer (QSCAT) data was stronger than those from Tropical Atmosphere Ocean (TAO) data and from National Centers for Environmental Prediction/National Center for Atmospheric Research (NCEP/NCAR) reanalysis I. As a result, the Intertropical Convergence Zone (ITCZ) in the Pacific Ocean is more southward in the QSCAT data than in the NCEP/NCAR data. Relative to the NCEP wind, the southern shift of the ITCZ in the QSCAT data led to negative anomaly of wind stress curl north of a latitude of 6°N. The negative anomaly results in downward Ekman pumping in the central Pacific. The excessive local strong easterly wind also contributes to the downward Ekman pumping. This downward Ekman pumping suppresses the thermocline ridge, reduces the meridional thermocline slope and weakens the North Equatorial Countercurrent (NECC). These effects were confirmed by numerical experiments using two independent ocean general circulation models (OGCMs). Furthermore, the excessive equatorial easterly wind stress was also found to contribute to the weaker NECC in the OGCMs. A comparison between the simulations and observation data indicates that the stronger zonal wind stress and its southern shift of QSCAT data in the ITCZ region yield the maximum strength of the simulated NECC only 33% of the magnitude derived from observation data and even led to a "missing" NECC in the western Pacific.

Key words: QuikSCAT, wind stress, NECC, ocean model, ITCZ

Citation: Wu, F. H., P. F. Lin, and H. L. Liu, 2012: Influence of a southern shift of the ITCZ from Quick Scatterometer data on the Pacific North Equatorial Countercurrent. *Adv. Atmos. Sci.*, **29**(6), 1292–1304, doi: 10.1007/s00376-012-1149-1.

1. Introduction

The North Equatorial Countercurrent (NECC) is a major component of the wind-driven circulation in the tropical Pacific. It is located at 5°N in the western Pacific and shifts northward to 7°N in the eastern Pacific according to the work of Donguy and Meyers (1996) and Johnson et al. (2002) and is closely tied to the meridional movement of the Intertropical Convergence Zone (ITCZ). The NECC is an eastward current against the prevailing trade winds, and its maximum speed reaches 40 cm s^{-1} near 140°W (Johnson et al., 2002). Because the NECC occurs at the transition regions between the equatorial gyre and the tropical gyre, it plays an important role in the wind-driven circulation in the tropical Pacific and its accurate simu-

*Corresponding author: LIN Pengfei, linpf@mail.iap.ac.cn

lation is consequential to many aspects of atmospheric and oceanic modeling.

According to classical theory, the strength of the meridional gradient of wind stress curl, namely $\mathrm{curl}_y\tau$, in the ITCZ controls the NECC transport (Sverdrup, 1947). An excessive zonal wind stress near the equator can also affect the NECC spatial pattern (Yu et al., 2000). Yu and Moore (2000) found that the strong zonal wind stress derived from the NASA Scatterometer (NSCAT) data in the ITCZ produces an upward Ekman pumping anomaly to the south and a downward anomaly to the north. These effects reduce the meridional slope of the thermocline and drive a weaker NECC. These studies have shown that the correctness of wind stress is one of the key factors in properly simulating the NECC.

In a sequential mission for the NSCAT, the Quick Scatterometer (QSCAT) has also provided oceanic surface wind measurements with much greater spatial and temporal coverage than any previous traditional observation method. QSCAT data can better describe the finer structures of surface wind fields (Chelton et al., 2004; Xie et al., 2001; Kessler et al., 2003). However, Kessler (2002) found that QSCAT drove a relatively weak NECC near 120°W. The simulated NECC in a high-resolution oceanic general circulation model (OGCM), forced by QSCAT wind stress (Sasaki et al., 2006), also showed weaker results than that forced by the NCEP reanalysis. Moreover, a comparison of the wind curl of Scatterometer Climatology of Ocean Winds (SCOW, which is derived from QSCAT) with that of the National Centers for Environmental Prediction (NCEP), Risien and Chelton (2008) showed a difference between alternating bands of negative and positive wind curl south of the ITCZ in the eastern Pacific. These bands may cause much weaker Sverdrup transport in the central-western tropical Pacific in the QSCAT than in the NCEP. According to these studies, simulations of the NECC forced by wind stress from satellites may have a relatively large bias in standalone oceanic models.

Because of the incomparability of spatial and temporal resolutions, QSCAT wind data has become a popular product used to force the OGCMs, especially high-resolution OGCMs. Therefore, the purpose of the present study was to further identify the distinctiveness of QSCAT wind data in the tropical Pacific and its effects on the NECC. We focused on whether QSCAT data can drive a reasonable NECC and the corresponding reasons. This paper is organized as follows: section 2 describes the datasets, OGCMs, and experiments used in this study, and section 3 compares wind stress datasets directly as well as the results from numerical experiments. Sverdrup transport and Ekman pumping velocities are provided to clarify the relationship of wind stress and the NECC. The effect of the equatorial forcing on the simulated NECC is also included. A brief summary and discussion are given in the last section.

2. Data and methods

2.1 *Data*

The QSCAT-derived monthly mean wind product used here on a global grid (0.5°×0.5° resolution) was provided by CERSAT (the Center for Satellite Exploitation and Research) at IFREMER (French Research Institute for Exploitation of the Sea) (IFREMER/CERSAT, 2002). Wind data from the NCEP/NCAR (National Center for Atmospheric Research) reanalysis 1 (NCEP), which has a spatial resolution of 1.875°, were used for comparison (cf., Kalnay et al., 1996; Kistler et al., 2001). Although the NCEP fields tend to have weaker stresses in the tropics than other wind products in the climatologically mean because of coarser resolution (Josey et al., 2002), the NCEP is one of the products most frequently used to force numerical OGCMs and these data overlap the time series of QSCAT. Therefore, we evaluated the annual mean QSCAT surface wind for 2000–2007 and compared it to the NCEP data during the same period. To assess the zonal wind stress near the equator and in the ITCZ, the oceanic surface wind stress vectors from the Tropical Atmosphere Ocean (TAO) project were used. These data were downloaded from the website http://www.pmel.noaa.gov/tao/oceansites/flux/main.html.

2.2 *Models and experimental design*

To capture common features while avoiding model-dependent conclusions, two OGCMs were employed in this study. One model was the LASG/IAP (State Key Laboratory of Numerical Modeling for Atmospheric Sciences and Geophysical Fluid Dynamics/Institute of Atmospheric Physics) Climate System Ocean Model (LICOM), which is an eddy-permitting, quasi-global model (75°S–65°N) with a uniform grid resolution of 0.5°. This model uses 30 vertical levels with 12 even levels in the upper 300 m. The vertical mixing scheme follows the Pacanowski and Philander (1981, hereafter PP) scheme used in LICOM. The scheme can be written as follows:

$$v = \frac{v_0}{(1+5Ri)^2} + v_\mathrm{b} \,, \tag{1a}$$

$$\kappa = \frac{\nu}{(1+5Ri)} + \kappa_\mathrm{b} \,, \tag{1b}$$

$$Ri = \frac{g}{\rho_0}\frac{\partial \rho}{\partial z} \Big/ \left[\left(\frac{\partial U}{\partial z} \right)^2 + \left(\frac{\partial V}{\partial z} \right)^2 \right], \qquad (1c)$$

where v is viscosity and κ is the diffusivity coefficient, v_0 is equal to 50 cm^2 s^{-1}, the background viscosity v_b is 1 cm^2 s^{-1}, and the diffusivity coefficient κ_b is 0.1 cm^2 s^{-1}. In addition, Ri is the bulk Richardson number; g is the gravity acceleration of seawater. Here ρ is the potential density of seawater; and U and V are the zonal and meridional velocities, respectively. More details can be reviewed in Liu et al. (2004).

The other OGCM used in this study was the Modular Ocean Model version 4 (MOM4, Griffes et al., 2005; Gnanadesikan et al., 2006), which was developed by the Geophysical Fluid Dynamics Laboratory (GFDL). This global model has a zonal grid resolution of 1°, with varying meridional resolution (extending from 1/3° at the equator to 1° poleward of 30°). The model uses 40 vertical levels with 20 even levels in the upper 200 m. Vertical viscosity and diffusivity are calculated using the K-profile parameterization (KPP) scheme (Large et al., 1994).

Forced by two climatological wind datasets from the QSCAT and the NCEP, both LICOM and MOM4 start with the same climatological temperature and salinity obtained from the World Ocean Atlas (WOA, Antonov et al., 1998). The sea surface temperature (SST) and sea surface salinity (SSS) were also restored to the WOA observation. All experiments were integrated for 50 years. In the simulation in tropics, the 20-year integration almost reached balance. Therefore, the 50-year integration is long enough for the tropics. Results from the last 10 years of the integration were used for analyses. The current velocity from Johnson et al. (2002) and the temperature from the WOA were used to evaluate the model results. To distinguish the position of ITCZ, we used the annual mean rate of rainfall, which was provided by Tropical Rainfall Measuring Mission (TRMM, Senior Review Proposal retrieved from http://trmm.gsfc.nasa.gov/trmm_rain/Events/TRMMSenRev2007_pub.pdf).

We first compared the annual mean QSCAT wind against the reanalysis dataset from the NCEP and observation data from the TAO. Then the results of the four experiments using the two different OGCMs forced by QSCAT and NCEP wind stress datasets were compared with the theoretical diagnosis and observation data.

3. Results

3.1 *Wind stress and wind curl*

The annual averaged wind stress derived from the QSCAT data was significantly different from that derived from the NCEP data in the tropical Pacific (vec-

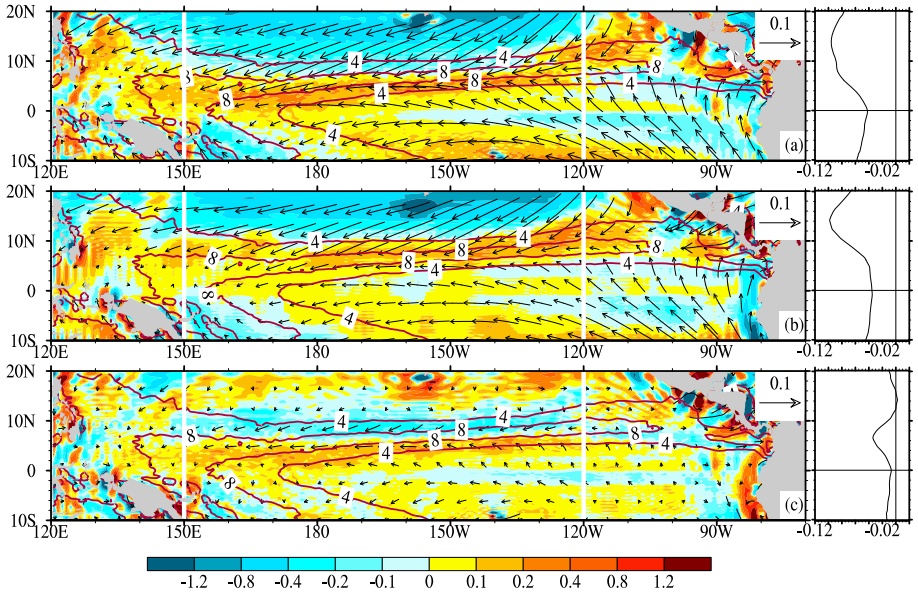

Fig. 1. Annual mean wind stress (vectors, N m^{-2}) and wind stress curl (shaded interval: 0.1×10^{-7} N m^{-3}) for (a) the QSCAT data, (b) the NCEP data and (c) the difference between the QSCAT and NCEP data (QSCAT-NCEP). The zonal mean of zonal wind stress between 150°E and 120°W (black straight lines) and its difference are shown on the right panels. The red contour is annual mean TRMM rain rate (contours interval: 4 mm d^{-1}).

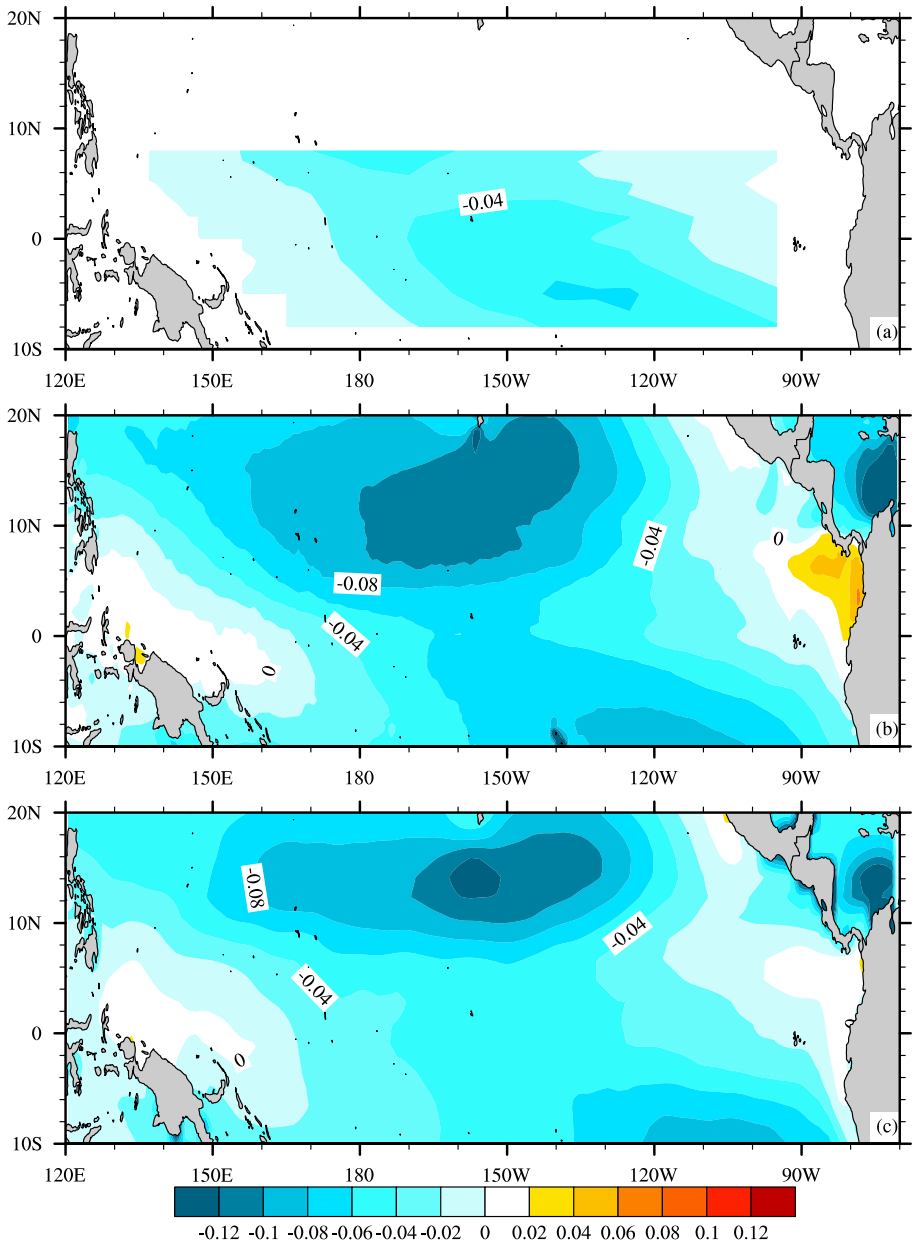

Fig. 2. Annual mean zonal wind stress for (a) the TAO data, (b) the QSCAT data, and (c) the NCEP data. The shaded interval is 0.02 N m^{-2}.

tors shown in Figs. 1a and b). The northeast and southeast wind stresses were stronger in the QSCAT data than in the NCEP data in the northern and southern Pacific, respectively, as revealed by their differences (vectors shown in Fig. 1c). The strong northeast and southeast wind stress is mainly due to their strong zonal components. According to Fig. 1, the easterly wind stress in the QSCAT data was stronger than that in the NCEP data, especially in the region between 0°–10°N and 150°E–120°W. Figure 2 presents the annual mean zonal wind stress derived from TAO, QSCAT, and NCEP datasets. Significant quantitative differences can be seen in the equatorial Pacific. The easterly for QSCAT exceeds 0.06 N m^{-2} in the central equatorial Pacific, while it is approximately 0.03 N m^{-2} for TAO. However, the easterly for the NCEP data is closer than that for the TAO data than that for the QSCAT data in this region. In the eastern equatorial Pacific Ocean, the westerly for QSCAT is also stronger than both TAO and NCEP.

The northeasterly and southeasterly trade wind belts converge in the ITCZ where the rainfall rate is

high. Here we used the TRMM rain rate; the highest rain rate represents the center of the ITCZ (red lines in Fig. 1). In the center of the ITCZ, the magnitude of wind stress should be the minimum. The easterly wind stress minimum in the NCEP data matches the highest rain rate. At the same time, the latitude of the easterly minimum in the QSCAT data is more southward than the position of highest rain rate and that in the NCEP data (Figs. 1a and b), which is also displayed in its zonal averaged profile (Fig. 1 plots) and zonal wind stress (Fig. 2). This indicates a southward shift of the ITCZ in the QSCAT data. Due to this shift, the maximal easterly difference (approximately -0.04 N m^{-2}) is located between 5°N and 7°N, i.e., in the ITCZ region (Fig. 1c).

We compared the QSCAT data with the TAO data to identify the magnitudes of zonal wind stress. The two latitude belts are plotted in Fig. 3. The near-equatorial easterly wind stress of the NCEP data and the QSCAT data are stronger than those of the TAO data (Fig. 3a). The deviation of a 0.02 N m^{-2} of the TAO data from the QSCAT data is larger than that for the NCEP data. Meanwhile, in the ITCZ region, the strength of easterly wind stress of the QSCAT data is twice that of the TAO data and the NCEP data (Fig. 3b). Moreover, the deviation from the TAO data for the QSCAT data is the largest in the central Pacific, both in the near-equatorial and the ITCZ regions.

The magnitude difference of the easterly associated with the ITCZ southward shifting results in the change of meridional gradient of wind stress. Furthermore, it affects the wind stress curl pattern because the meridional gradient is the dominant term for wind stress curl in the tropical Pacific. Generally, the positive curl lies at ITCZ, while the negative curl is located north of ITCZ and eastern equatorial Pacific Ocean in the two wind products (Fig. 1, shaded area). However, north of the equator, the position of zero wind curl in the QSCAT shifts southward. The difference of the ITCZ location between the QSCAT and the NCEP results in a cross-basin band of the negative and positive anomalies of wind curl on both sides of about 6°N (i.e., in the ITCZ): negative north and positive south (shaded, Fig. 1c), respectively.

Wind-driven currents dominate in the tropical Pacific. Therefore, the differences of wind stress curl affect the simulated currents and temperature in the tropical Pacific. The results are presented in the following sections.

3.2 *Simulation results*

To evaluate the effect of the southern shift of the ITCZ on the magnitude of the equatorial currents and the structure of temperatures associated with currents in the tropical Pacific, four numerical experiments were conducted using two different OGCMs, LICOM and MOM4, forced by the climatological wind stress of the QSCAT data and the NCEP data (using the same period: 2000–2007). The black contours in Figs. 4a and b show the simulated zonal currents along 140°W in LICOM forced by surface wind from the QSCAT data and the NECP data, respectively. The most significant differences in the zonal current between the two experiments occur north of 6°N. Both the NECC and north equatorial current (NEC) are weak when forced by the QSCAT data. The magnitude of the

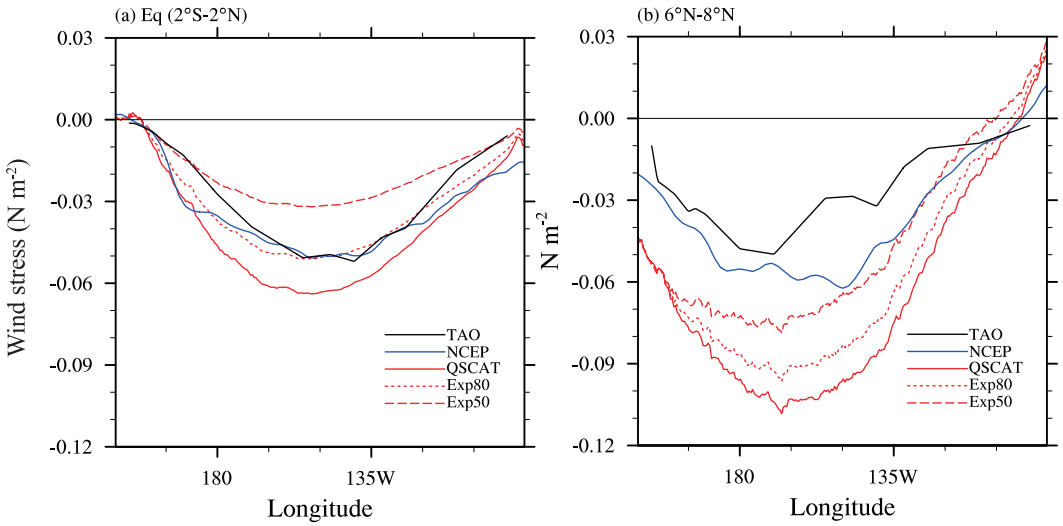

Fig. 3. The mean zonal wind stress (N m^{-2}) near the equator: (a) averaged from 2°S to 2°N and in the ITCZ region and (b) averaged from 6°N to 8°N. The Tropical Atmosphere Ocean (TAO) wind stress was calculated according to surface wind downloaded from http://www.pmel.noaa.gov/tao/oceansites/flux/main.html.

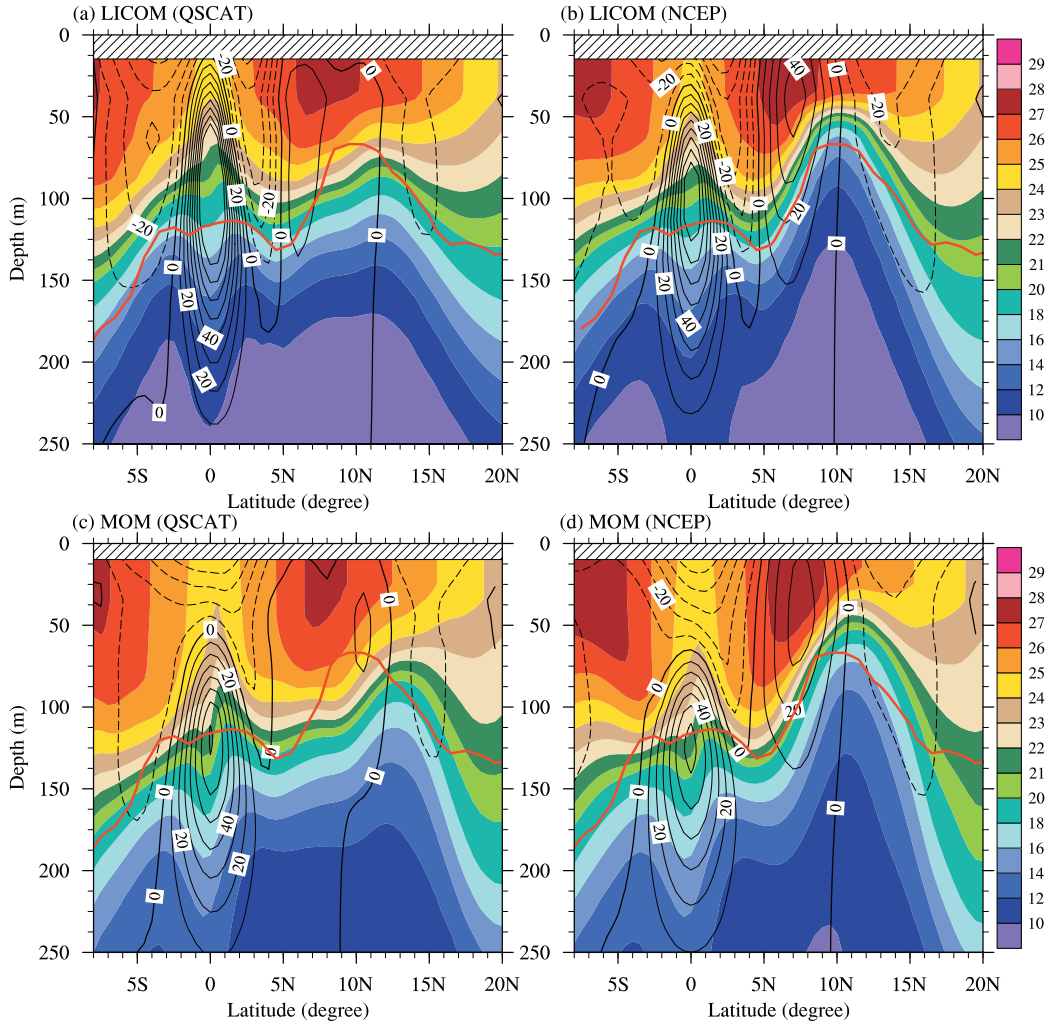

Fig. 4. The latitude–vertical distribution of simulated zonal currents (black contours, positive is eastward, contour interval: 10 cm s^{-1}) and oceanic temperature (shaded interval: 1°C) along 140°W. The contour interval is 10 cm s^{-1}. Panels (a) and (b) are for LICOM forced by the QSCAT data and the NCEP data, respectively. Panels (c) and (d) are the same as panels (a) and (b), but for MOM. The red curves are annual mean 20°C isotherm from the WOA.

NEC in the QSCAT run is approximately half that of the NCEP run. The NECC in the QSCAT run is located slightly toward the equator. The NECC maximum is nearly 10 cm s^{-1} in the QSCAT run, while it is as much as 30 cm s^{-1} in the NCEP run.

Another difference can be found in the simulated thermocline, which is represented by a 20°C isotherm in this study (shaded in Figs. 4a and b). It is evident that the ridge of the thermocline around 10°N is much deeper in the QSCAT run than in the NCEP run. The deep thermocline ridge in the QSCAT run reduces meridional thermocline gradient on the both sides, which is associated with the weak surface zonal current. The experiments conducted by MOM4 show similar simulated differences forced by two wind data in the Northern Hemisphere, especially with regard to the weak velocity of the NECC and its related structure of thermocline ridge in the QSCAT run (Figs. 4c and d). These results further confirm the simulation results of LICOM.

To inspect the differences of the NECC and NEC forced by two different winds, we compared the simulated barotropic stream functions (shaded in Figs. 5a and b). The surface wind from the QSCAT data forces a weak southern shift of anti-clockwise circulation north of the equator. This results in a large positive anomaly between 6°N and 14°N and a large negative anomaly between 0°N and 6°N (Fig. 5c). The band

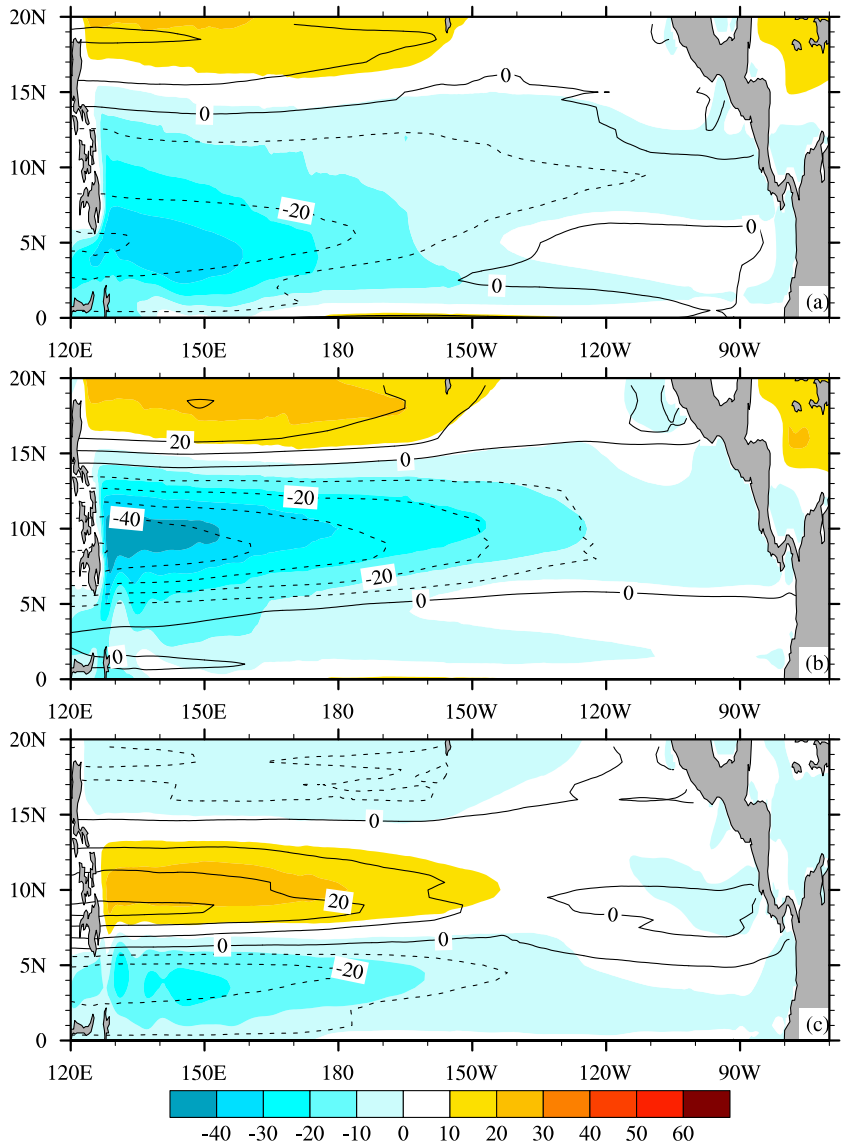

Fig. 5. The stream function of Sverdrup transport (contour interval: 10 Sv, 1 Sv=10^6 m^3 s^{-1}) calculated by Sverdrup theory and barotropic stream function (shaded interval: 10 Sv) for (a) the QSCAT run, (b) the NCEP run and (c) the difference between the QSCAT and NCEP runs (QSCAT-NCEP).

of large positive (negative) anomaly of the barotropic stream function in the Northern Hemisphere is co-located with the band of negative (positive) anomaly of wind stress curl (Fig. 1c).

3.3 *Comparison with the observation*

The significant surface-wind difference between the QSCAT data and the NCEP data in the northern tropical Pacific was identified by both direct comparison with annual mean wind stress and the results from numerical experiments forced by the two datasets. However, we were not able to determine which simulation forced by two kinds of wind datasets more closely matched the observation data. To answer this question, we first compared the simulated thermocline with the observation data WOA. Here the 20°C isothermal depth is as a measure of thermocline. In Fig. 4, the red curves are the 20°C isothermal along 140°W from the WOA. In either LICOM or MOM4, the thermocline ridges in the Northern Hemisphere forced by surface wind stress from the NCEP are much closer to the observation compared with those forced by the QSCAT wind. The ridges shift northward and become weak in the experiments forced by the QSCAT data. The northern shift of the ridges is explained in the following section.

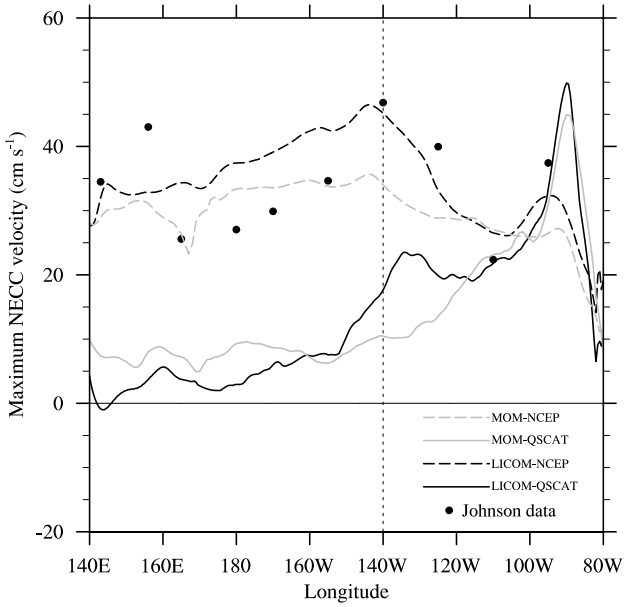

Fig. 6. The maximum zonal velocities (cm s^{-1}) between 3°N and 10°N within the upper 80 m for the work of Johnson et al. (2002, black dots), MOM forced by the NCEP data (grey dash), MOM forced by QSCAT data (grey solid), LICOM forced by the NCEP data (black dash) and LICOM forced by QSCAT data (black solid).

Second, the simulated NECCs were compared with observations with the work of Johnson et al. (2002). Figure 6 shows the maximal zonal currents between 3°N and 10°N for four numerical experiments (Fig. 6, curves) and the work of Johnson et al. (Fig. 6, dots). Because latitudes of the NECC vary with longitude, we used the maximum of the zonal currents between certain latitudes instead of the meridional averaged value. In the observation data (Johnson et al., 2002), the maximum values of zonal velocity between 3°N and 10°N at specified longitudes are nearly all larger than 20 cm s^{-1}. The NECC in the NCEP is within the observed range, while the NECC in the QSCAT is weaker than observation data from Johnson et al. (2002), especially in the western-central Pacific. It appears nearly absent in the central Pacific and even a "missing" flow in the western Pacific. The comparisons between the simulation and observation indicate that the simulated NECC and NEC driven by the NCEP are more realistic than those driven by the QSCAT in the central Pacific.

3.4 *Sverdrup transport and Ekman pumping velocity*

According to the classical Sverdrup theory, in the Northern Hemisphere the positive wind stress curl drives a northward transport and the negative wind stress curl drives a southward transport. For the QSCAT run, due to southern shift of ITCZ, the negative and positive anomalies of wind stress curl north and south of 6°N. Therefore, the anomalous convergence of the meridional transport produces downwelling, suppressing the thermocline ridge around 6°N. This results in weak NECs and NECCs in the QSCAT runs. Sverdrup transports are also computed for the QSCAT and NCEP data (contours in Figs. 5a and b). The pattern of Sverdrup transport matches that of simulated barotropic stream function. This comparison further indicates that the difference between the simulated currents (NECC and NEC) is primarily caused by the difference of surface wind stress curl.

The magnitude of difference between the simulated currents (NECC and NEC) can be explained by the difference of the Sverdrup transport. However, the detailed position of the current and thermocline could not be seen clearly. The following section presents the Ekman pumping velocity, through which the wind stress curl impacts the ocean directly. These effects explain how the wind stress produces the currents and thermocline locally.

Generally, the Ekman pumping velocity due to wind stress is defined as

$$w_{\mathrm{E}} = \mathrm{curl}_z \left(\frac{\tau}{\rho f} \right) , \qquad (2)$$

where τ is the wind stress, ρ is the density of seawater (take here as 1025 kg m^{-3}) and f is the Coriolis parameter. A positive value means upwelling, and a negative value means downwelling. Figure 7 presents the Ekman pumping velocity based on the two different wind datasets and their difference. Negative Ekman pumping velocities dominate in the central Pacific between 5°N to 10°N for the QSCAT (Fig. 7a), which suppresses the uplift of the thermocline and reduces the meridional thermocline slope and the NECC magnitude. Positive Ekman pumping is limited east of 130°W. However, for the NCEP (Fig. 7b), there is a positive Ekman pumping velocity from the western to eastern Pacific between 5°N to 10°N. On both meridional sides of the positive velocity, negative velocities dominate. The positive and negative velocity induces upwelling and downwelling, respectively. Thus, on both meridional sides of the positive velocity, the meridional thermocline slopes increase, which strengthens the NECC and NEC in the central Pacific forced by the NCEP wind stress. As illustrated by the difference in Ekman pumping velocity (Fig. 7c), there are negative anomalies between 5°N to 10°N in the central Pacific. They suppress the uplift of thermocline locally and reduce the meridional thermocline slope on both meridional sides of negative anomalies,

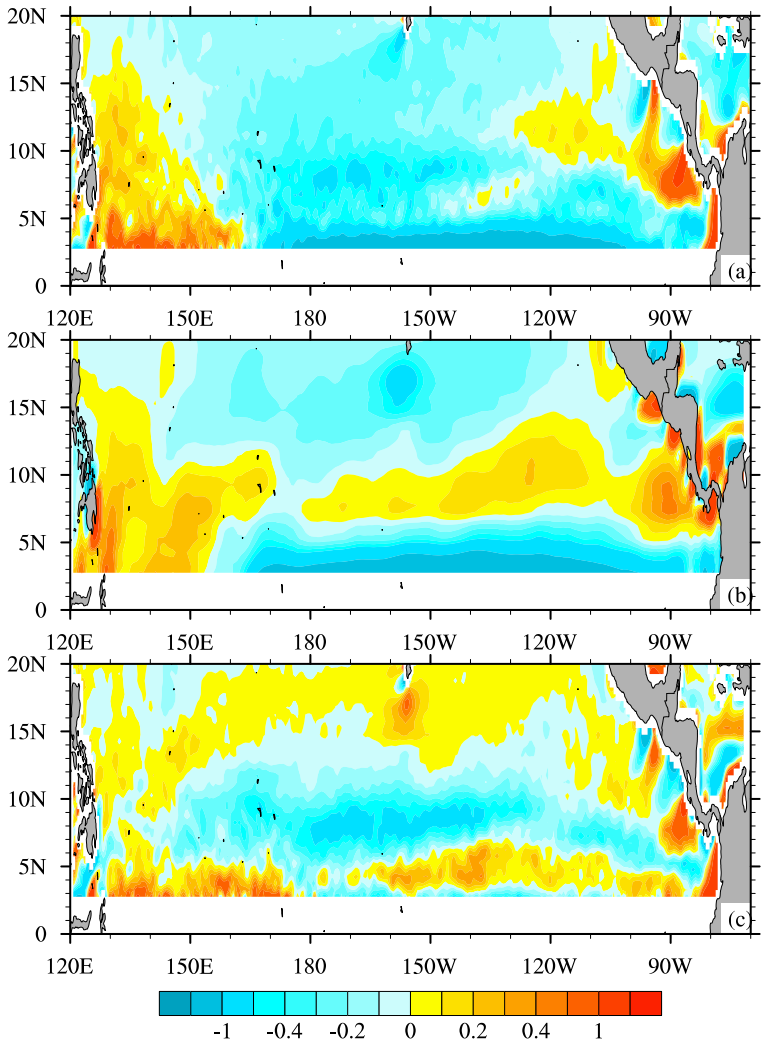

Fig. 7. Ekman pumping velocity (shaded interval: 0.1×10^{-5} m s^{-1}) for (a) the QSCAT, (b) the NCEP, and (c) the difference between the QSCAT and NCEP (QSCAT-NCEP). Ekman pumping velocity is not plotted south of 2°N because it is singular near the equator.

which gives rise to weak NECC and NEC for the QSCAT run in the central Pacific.

In the eastern Pacific, the positive Ekman pumping velocity for the QSCAT occur around 10°N and shifts southward to 6°N from 130°W to 85°W, which induces the uplift of thermocline and leads to a strong NECC. Thus, the simulated NECC in the eastern Pacific (east of 130°W) is well captured by the QSCAT forcing compared to observation data from Johnson et al. (2002) (Fig. 6).

Furthermore, the Ekman pumping velocity in the previous equation can be decomposed into two terms:

$$\mathrm{curl}_z\left(\frac{\tau}{\rho f}\right) = \left(\frac{1}{f}\right)\mathrm{curl}_z\left(\frac{\tau}{\rho}\right) + \left(\frac{\beta}{f^2}\right)\left(\frac{\tau^x}{\rho}\right), \quad (3)$$

where β is the meridional derivative of the Coriolis parameter. The first term from the right-hand side (RHS) of Eq. (3) is related to the wind stress curl. The second term of the RHS is proportional to zonal wind stress τ^x and $1/f^2$, which become relatively important near the equator. Because the easterly wind blows consistently in the central Pacific, the second term always leads to downward Ekman pumping. Thus, the upward Ekman pumping is only due to the first term from the RHS of Eq. (3). Figure 8 presents Ekman pumping velocities according to the two terms from the RHS of Eq. (3). The large positive velocity (Fig. 8a) for the QSCAT is located south of the ITCZ, which is more southward than for the NCEP (Fig. 8b) in the central Pacific and is close to the equator. The position difference is mainly due to the southward shift of large positive wind stress curl for the QSCAT (Fig. 1),

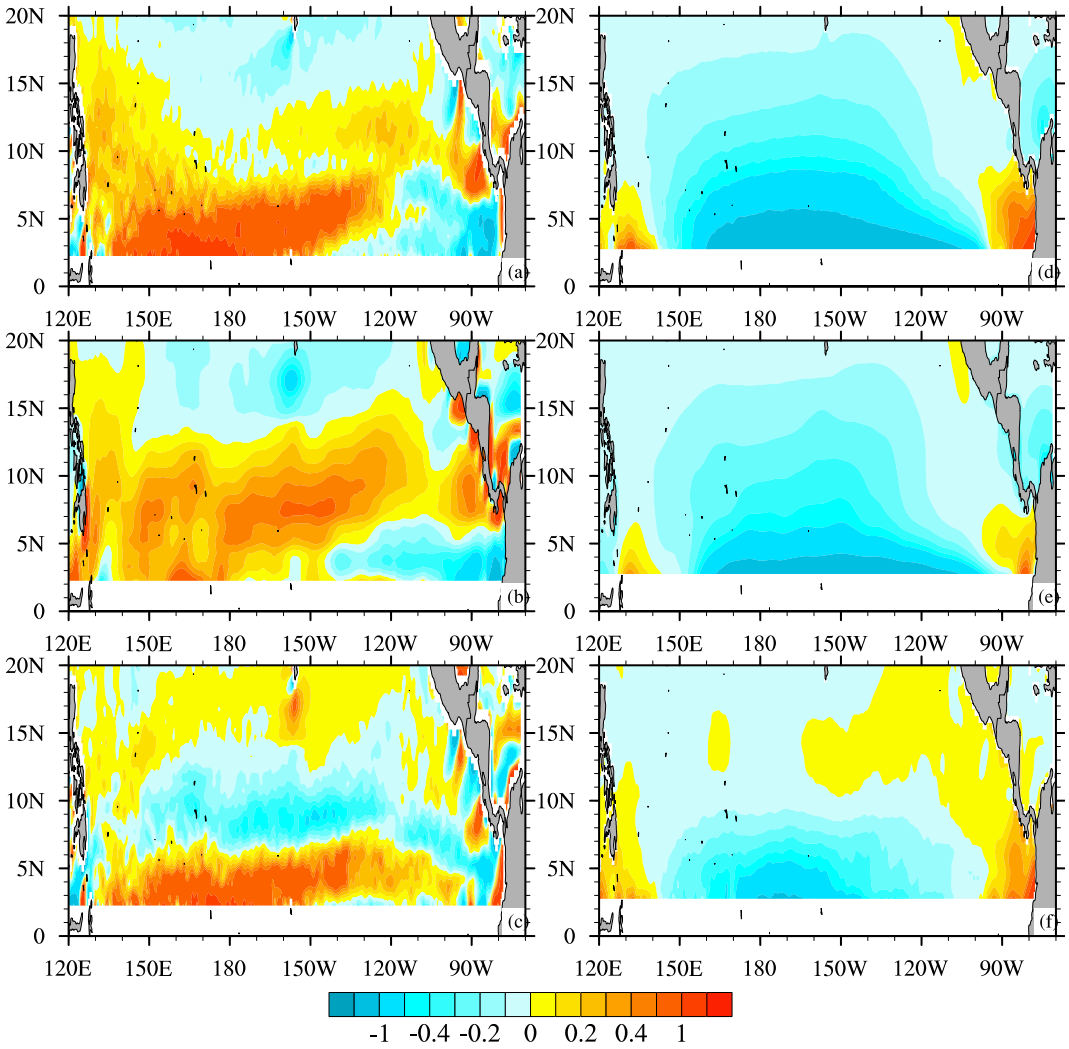

Fig. 8. Ekman pumping velocity related to wind stress curl (shaded interval: 0.1×10^{-5} m s^{-1}) for (a) the QSCAT, (b) the NCEP, (c) the differences between the QSCAT and NCEP (QSCAT-NCEP). Ekman pumping velocity related to zonal wind stress (shaded, in 10^{-5} m s^{-1}) for (d) the QSCAT, (e) the NCEP, (f) the differences between the QSCAT and NCEP (QSCAT-NCEP).

which can result in negative velocity anomalies in the ITCZ relative to the NCEP (Fig. 8c). In addition, the magnitude of the positive center value exceeds that of the NCEP at the equator.

Because the easterly wind stress of the QSCAT run is stronger than that of the NCEP (Fig. 1) in the tropical Pacific, the magnitude of negative velocity due to the second term in the RHS of Eq. (3) for the QSCAT (Fig. 8d) is larger than in the NCEP (Fig. 8e). Although the difference in easterly wind stress is largest around 6°N, the difference in velocity (Fig. 8f) is largest near 2°N due to a small f. Comparing the difference of Ekman pumping velocity (Fig. 7c) with the differences (Figs. 8c and e) due to each term from the RHS of Eq. (3), both terms contribute to the negative Ekman pumping anomalies in the ITCZ between 6°N and 10°N in the central Pacific. However, south of 6°N, only the first term of the RHS of Eq. (3) contributes the positive Ekman pumping anomaly. Thus, the differences of both easterly wind stress and wind stress curl affect the negative Ekman pumping velocity anomalies in the ITCZ.

Along 140°W, positive velocities are located between 5°N and 10°N for the NCEP. This induces upward pumping and uplift of the thermocline around 10°N (Fig. 4a), which increases the meridional thermocline slope between 5°N and 10°N and strengthens the NECC. For the QSCAT, although the velocity is negative at 140°W in the ITCZ, the small positive velocity is around 130°W and the large positive value is east of 130°W north of 12°N. The effect is the uplifting of the thermocline east of 130°W. The vertical

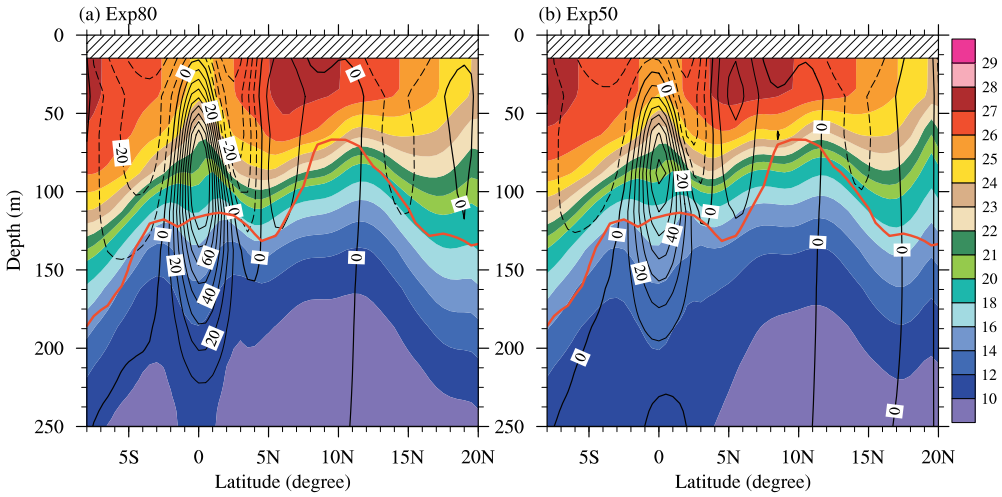

Fig. 9. Same as Fig. 4 except for (a) Exp80 and (b) Exp50, respectively. The experiments are based on LICOM.

temperature anomalies may be transported to 140°W by a westward Rossby wave forced by wind stress curl in this latitude and induce a weak uplift of the thermocline at 140°W. This produces a weak NECC. Thus, for the QSCAT run, the thermocline ridge shifts more northward than in the NCEP run.

3.5 *Effect of equatorial wind stress on NECC*

The analyses in the previous section focused on the effects of the local wind stress and its curl on the simulated NECC. The southward shift of the ITCZ in the QSCAT run reduces the thermocline slope in the ITCZ region and reduces the magnitude of the NECC. The equatorial zonal stress is stronger for the QSCAT run than for the NCEP run (Fig. 1c). The numerical experiments of previous studies have shown that the near-equatorial zonal wind stress can affect the spatial structure continuity of NECC near the dateline (Yu et al., 2000). To check the effect of equatorial zonal wind stress on the NECC, we designed the following two extra experiments using LICOM. The zonal wind stress between 20°S and 20°N for the QSCAT were reduced to 80% (Exp80) and 50% (Exp50) of the averaged zonal wind stress near the equator (from 2°S to 2°N), respectively. Both experiments were run for a simulation time of 20 years. The initial values of these two experiments were the same as those for the original four experiments. The last 5 years of the integration were used for analysis. Although the zonal wind stress in these two runs were reduced, the meridional gradient of the wind stress curl ($\mathrm{curl}_y\tau$) remained unchanged in the ITCZ because altered zonal wind stress did not change the meridional gradient between 20°S and 20°N. These results provide insight into the effect of zonal wind stress near the equator on the NECC. Although the modified zonal wind stress changed the ($\mathrm{curl}_y\tau$) around 20°S/N, the simulated results within the latitude of 15°N were not affected.

The modified near-equatorial zonal wind stress is shown in Fig. 3a (red dotted and dashed lines). The equatorial easterly wind stress is closer to the TAO and the NCEP when the value is reduced by 20% in Exp80. In the ITCZ region, both modified zonal wind stress remain stronger than in the TAO and NCEP. The simulation results forced by changed zonal wind stress are presented in Fig. 9. Compared with the QSCAT run, the simulated NECC strengthens only slightly along 140°W in the Exp80 run (Fig. 9a) but strengthens substantially in the Exp50 run (Fig. 9b). The positions of the maximal NECC magnitude in the Exp80 and Exp50 runs remain located at 6°N and do not change relative to the original QSCAT run. This result may be related to the southern shift of wind stress curl for the QSCAT. The temperature ridge around 6°N is uplifted in the Exp50 run relative to the QSCAT run. This increases the meridional thermocline slope and strengthens the NECC. Compared with observation data from Johnson et al. (2002), after reducing the near-equatorial zonal wind stress, the maximal magnitude of the NECC in the Exp50 run is strengthened. These experiments show that the magnitude of near-equatorial zonal wind stress can impact not only the spatial structure of the NECC (Yu et al., 2000) but also the NECC strength.

4. Discussion and conclusion

The results of this study show that the easterly wind stress for the QSCAT data in the northern tropical Pacific Ocean is stronger than those of the TAO

data and the NCEP data. The ITCZ in the QSCAT data shifts southward in the central Pacific. Compared with the NCEP, the southern shift of the ITCZ in the QSCAT data leads to a band of negative and positive wind stress curl anomalies on both sides surrounding 6°N (i.e., in the ITCZ): negative north and positive south. The negative anomaly results in anomalous downward Ekman pumping in the central Pacific. The excessively local strong easterly wind stress around the ITCZ region also contributes to the downward anomalies. Both suppress the thermocline ridge there and reduce the meridional thermocline slope and magnitude of the NECC in the central Pacific. East of 130°W in the eastern Pacific, the upward Ekman pumping for the QSCAT can uplift the thermocline ridge, which is associated with a reasonable stronger NECC. These effects were confirmed by numerical experiments using two different OGCMs. Furthermore, the excessive easterly wind stress near the equator reduces the magnitude of the NECC by sensitive experiments. The comparison between the simulations and observation data from the WOA and the work of Johnson et al. (2002) indicates that the pattern of wind stress and its curl for the QSCAT run in the ITCZ region yields the weak simulated NECC and the deep thermocline. This bias of QSCAT data impacts the simulated equatorial gyre and the tropical gyre in the Pacific.

Yu and Moore (2000) found stronger easterly wind stress derived from the NSCAT data in the latitude band of the ITCZ. The excessively easterly was associated with distorted Ekman pumping across the ITCZ band, which reduced the thermocline slope in the ITCZ region and subsequently reduced the magnitude of the NECC. According to our analyses, the weak NECC forced by the QSCAT data is related to small upward Ekman pumping in the ITCZ region, which in fact is mainly due to the southern shift of the ITCZ. The shift causes a large positive Ekman pumping velocity to locate south of the ITCZ rather than north of the center of the ITCZ. Moreover, an excessive local easterly produces an excessive downward pumping. Thus, the total Ekman pumping is downward north of the center of the ITCZ. This effect suppresses the uplift of the thermocline and reduces the magnitude of the NECC. Meanwhile, the small magnitude of the simulated NECC can also be forced by an excessive easterly wind stress near the equator for the QSCAT data.

In this study, we limited our focus to the NECC in the tropical Pacific. In fact, the wind stress and its curl also impact other currents in the tropical Pacific, such as the southern equatorial current (SEC), the equatorial undercurrent (EUC), and the northern equatorial current (NEC). Using two OGCMs with different horizontal resolutions and physical parameter schemes, the differences of simulated NEC, NECC, SEC, and EUC between the NCEP runs and QSCAT runs were similar in LICOM and MOM4. For instance, the simulated south branch of the SEC was better captured when forced by QSCAT wind than when forced by the NCEP both in the LICOM and MOM4. This is similar to that of Sasaki et al. (2006), and it implies that the simulated oceanic currents in the tropical Pacific that are forced with different wind fields are mainly traceable to the difference in wind stress. Although there were simulated differences between both models forced by the same wind stress, such as the position and magnitude of the EUC, these effects were outside the scope of this study and they should be studied further. In this study, we primarily focused on the effect of wind stress and its curl on the NECC. In addition, only the dynamical part of wind stress was analyzed, and the thermal part (which impacts heat flux by altering wind speed) will be analyzed in our future work.

The distinctiveness of QSCAT surface wind stress and its effect on NECC have been identified. In our next study, we will discuss the causes of the error in the QSCAT surface wind. As we know, the QSCAT surface wind vector is retrieved from the radar backscatter signal by an empirical model function. However, it is contaminated by heavy rain. Consequently, there are missing values or large uncertainties in heavy rain regions such as the ITCZ region (Milliff et al., 2004). Yu and Moore (2000) also pointed out that in the QSCAT predecessor, the NSCAT, bias was due to the rain rate. However, additional discussion about the causes of the error in the QSCAT surface wind is beyond the scope of this study.

Notably, in this study we chose only the NCEP wind data for comparison with QSCAT data because ERA40 does not cover the entire period of QSCAT (2000–2007) and because NCEP2 is considered to be similar to NCEP1 in the tropical Pacific (Ebisuzaki et al., 1998; Risien and Chelton, 2008). In future research, we will systematically compare QSCAT with other reanalysis products, such as MERRA (Modern-Era Retrospective Analysis for Research and Applications) and NCEP CFSR (Climate Forecast System Reanalysis).

Acknowledgements. The authors appreciate the constructive comments given by Prof. ZHANG Xuehong and YU Zuojun. The authors gratefully acknowledge the valuable comments made by anonymous reviewer. We appreciated that TAO Project provided surface wind data on the website. This work was jointly supported by the National Basic Research Program of China (Grant Nos. 2010CB428904 and 2010CB950502), the Natural Science

Foundation of China (Grant Nos. 40806007 and 40906012), an open project of LAPC-KF-2008-05, Program of Excellent State Key Laboratory No. 41023002 and National High Technology Research and Development Program of China (Grant No. 2010AA012303).

REFERENCES

Antonov, J. I., S. Levitus, T. P. Boyer, M. E. Conkright, T. D. O'Brien, and C. Stephens, 1998: Temperature of the Atlantic Ocean. Vol. 1, *World Ocean Atlas 1998*, NOAA Atlas NESDIS 27, 166pp.

Chelton, D. B., M. G. Schlax, M. H. Freilich, and R. F. Milliff, 2004: Satellite radar measurements reveal short-scale features in the wind stress field over the world ocean. *Science*, **303**, 978–983.

Donguy, J., and G. Meyers, 1996: Mean annual variation of transport of major currents in the tropical Pacific Ocean. *Deep-Sea Res. I*, **43**, 1105–1122.

Ebisuzaki, W., M. Kanamitsu, J. Potter, and M. Fiorino, 1998: An overview of Reanalysis-2. *Proc. 23rd Climate Diagnostics and Prediction Workshop*, Miami, FL, Oct. 26–30.

Gnanadesikan, A., and Coauthors, 2006: GFDL's CM2 global coupled climate models, Part II: The baseline ocean simulation. *Journal of Climate*, **19**, 675–697.

Griffes, S. M., and Coauthors, 2005: Formulation of an ocean model for global climate simulations. *Ocean Science*, **1**, 45–79.

IFREMER/CERSAT, 2002: QuikSCAT scatterometer mean wind field products user manual. C2-MUT-W-04-IF, version 1.0, IFREMER/CERSAT, Plouzane, France, 47pp.

Josey, S. A., E. C. Kent, and P. K. Taylor, 2002: Wind stress forcing of the ocean in the SOC climatology: Comparisons with the NCEP-NCAR, ECMWF, UWM/COADS, and Hellerman and Rosenstein datasets. *J. Phys. Oceanogr.*, **32**, 1993–2019.

Johnson, G. C., B. M. Sloyan, W. S. Kessler, and K. E. McTaggart, 2002: Direct measurements of upper ocean currents and water properties across the tropical Pacific during the 1990s. *Progress in Oceanography*, **52**, 31–61.

Kalnay, E., and Coauthors, 1996: The NCEP/NCAR 40-Year Reanalysis Project. *Bull. Amer. Meteor. Soc.*, **77**, 437–471.

Kistler, R., and Coauthors, 2001: The NCEP-NCAR 50-Year Reanalysis: Monthly means CD-ROM and documentation. *Bull. Amer. Meteor. Soc.,* **82**, 247–268.

Kessler, W. S., 2002: Mean three-dimensional circulation in the northeast tropical Pacific. *J. Phys. Oceanogr.*, **32**, 2457–2471.

Kessler, W. S., Gregory C. Johnson, and D. W. Moore, 2003: Sverdrup and nonlinear dynamics of the Pacific equatorial currents. *J. Phys. Oceanogr.*, **33**, 994–1008.

Large, W. G., J. C. McWilliams, and S. C. Doney, 1994: Oceanic vertical mixing: A review and a model with a nonlocal boundary layer parameterization. *Rev. Geophys.*, **32**, 363–403.

Liu, H. L., X. H. Zhang, W. Li, Y. Q. Yu, and R. C. Yu, 2004: An eddy-permitting oceanic general circulation model and its preliminary evaluation. *Adv. Atmos. Sci.*, **21**(5), 675–690, doi: 10.1007/BF02916365.

Milliff, R. F., J. Morzel, D. B. Chelton, and M. H. Freilich, 2004: Wind stress curl and wind stress divergence biases from rain effects on QSCAT surface wind retrievals. *J. Atmos. Oceanic Technol.*, **21**, 1216–1231.

Pacanowski, R., and S. G. H. Philander 1981: Parameterization of vertical mixing in numerical models of tropical oceans. *J. Phys. Oceanogr.,* **11**, 1443–1451.

Risien, C. M., and D. B. Chelton, 2008: A global climatology of surface wind and wind stress fields from eight years of QuikSCAT Scatterometer data. *J. Phys. Oceanogr.*, **38**, 2379–2413.

Sasaki, H., Y. Sasai, M. Nonaka, Y. Masumoto, and S. Kawahara, 2006: An eddy-resolving simulation of the quasi-global ocean driven by satellite-observed wind field. *Journal of the Earth Simulator*, **6**, 35–49.

Sverdrup, H. U., 1947: Wind-driven currents in a baroclinic ocean; with application to the equatorial currents of the eastern Pacific. *Proceedings of the National Academy of Sciences of the United States of America,* **33**, 318–326.

Xie, S.-P., W. T. Liu, Q. Liu, and M. Nonaka, 2001: Far-reaching effects of the Hawaiian Islands on the Pacific ocean-atmosphere system. *Science*, **292**, 2057–2060.

Yu, Z., and D. W. Moore, 2000: Validating the NSCAT winds in the vicinity of the Pacific intertropical convergence zone. *Geophys. Res. Lett.*, **27**(14), 2121–2124, doi: 10.1029/1999GL011250.

Yu, Z., J. P. McCreary, W. S. Kessler, and K. A. Kelly, 2000: Influence of equatorial dynamics on the Pacific north equatorial countercurrent. *J. Phys. Oceanogr.*, **30**, 3179–3190.